Funded by the European Union

Transboundary Storm Risk and Impact Assessment in Alpine Regions

HAZARD SET – UNDER CLIMATE CHANGE

REVISION n.: 1	DATE: 31/05/2022	
DISSEMINATION LEVEL: Consortium	WP: 2	TASK(s): 2.3
AUTHORS:	Sebastian Lehner, Katharina Enigl, Klaus Haslinger	

Project duration: January 1st 2021 – December 31st 2022 (24 Months)

eurac research
arpav Agenzia Regionale per la Prevenzione e Protezione Ambientale del Veneto
BFW.
ZAMG Zentralanstalt für Meteorologie und Geodynamik

TABLE OF CONTENTS

1. INTRODUCTION

Extreme weather events and corresponding natural hazards have always been a major threat to people all over the globe. By now, it is common scientific consensus that climate change comes along with increases in both frequency and intensity of extreme weather events (IPCC, 2014; Feyen, 2012). Consequently, this development entails increasing amounts of associated natural hazard events (EEA, 2016). This poses a major challenge for decision-makers in the field of civil protection who are in need of an integrated multi-hazard storm risk assessment and impact forecasting methodology tailored to their needs.

In Deliverables 2.1 and 2.4, we put the focus on the identification of potentially damage-inducing weather sequences (so-called "Hazard Trigger Patterns", HTPs) and their potential change in frequency under different climate scenarios (so-called "Hazard Development Corridors", HDCs). Both were calculated for different hazard categories, i.e., floods and mass movements, in two regions, i.e., East Tyrol – Carinthia as well as South Tyrol, except for HDCs in South Tyrol, which were left out due to limited amounts of data. For the purpose of HTPs and HDCs, we intersected damage events that are precisely located in space and time with gridded meteorological data. However, we solely incorporated precipitation data in our analyses. Additional parameters that may contribute to the initiation of an event like e.g., vegetation or ground conditions have not been considered.

The first focus of this deliverable is the completion of "Hazard Development Corridors" (HDCs). These depict the changes in occurrence of respective HTPs for different hazard categories as well as in investigated regions. HDCs for South Tyrol are added and the previous delivered HDCs from D2.4 extended with more data.

For the second part of this deliverable, we aim at linking the synoptic scale weather situation to registered damages in the target regions and investigate potential changes under different climate scenarios. Therefore, we identify the prevailing weather type for each day since 1961, using the ERA5 reanalysis data (C3S, 2017; Hersbach et al., 2020). By intersecting locally recorded damage events with the prevailing weather type on the synoptic scale, we determine weather types that carry a higher potential of causing damage-inducing, or high-impact weather. Subsequently, we identify weather types in future climate scenarios on a daily basis in order to evaluate changes in frequency and intensity of those high-impact weather types. For the former, we can simply look at the changing distribution of weather types and assume a linear relationship between increasing weather type occurrence and increasing potential of high-impact weather events. For the latter, we also investigate on how different precipitation indicators change for specific weather types, especially for those that are connected to high-impact weather events. We furthermore lay special emphasis on Vaia and use the corresponding weather types as proxy on how "Vaia"-like events could potentially change.

In order to conduct stochastic simulations for "Vaia"-like events, there is a need to determine the boundary conditions, like the prevailing large-scale weather situation, as well as a plausibility check to which extent such simulations can be performed. In this deliverable we describe the large-scale weather situation and also investigate possible changes for large-scale weather types that were associated with Vaia. The weather types therefore act as a proxy for "Vaia"-like conditions. However, due to the coarse resolution of GCMs, it is not feasible to study regional trigger conditions for "Vaia"-

like events to the extent of explicit stochastic simulations on a regional scale. Hence, the presented results reflect the large-scale weather situation as a proxy for “Vaia”-like events as a needed pre-requisite, that can, but not necessarily always will, trigger devastating, high-impact weather events.

2. Data

○ Reanalysis data

ERA5 is a global reanalysis dataset with hourly weather data from 1950 until present in 31 km horizontal spatial resolution. It is updated regularly with a delay of 3 months. ERA5 has been developed by ECMWF Copernicus Climate Change Service (C3S) since 2016 and is available as open data. It is the successor of ERA-Interim (C3S, 2017; Hersbach et al., 2020).
It comprises a plethora of atmospheric variables on different pressure levels as well as on the surface level. In the context of this deliverable, we solely use “mean sea level pressure” for the identification of different weather types relevant for Europe at the synoptic scale.

○ GCM data

GCM data were taken from the CMIP6 (Coupled Model Intercomparison Project Phase 6) and follow the categorization into SSPs (Shared Socioeconomic Pathways). The four main scenarios of CMIP6 are SSP1-2.6, SSP2-4.5, SSP-3.70, SSP5-8.5. In this study, the two scenarios SSP1-2.6 and SSP3-7.0 are considered, representing a climate-friendly and a carbon fossil fuel intensive scenario, respectively. The first digit represents the socio-economic scenario (SSP1 for sustainability, SSP2 for the "middle of the road" path, SSP3 for regional rivalries, SSP5 for fossil development) and the last two numbers represent the considered RCP (“Representative Concentration Pathway”) indicating the radiative forcing in W/m². A comparison between SSP scenarios and the RCP scenarios known from CMIP5 can be found in Deliverable 2.4 and refers to Riahi et al., 2016. The use of the aforementioned SSP scenarios (SSP1-2.6, SSP3-7.0) covers a plausible range of potential future developments.
For the purpose of weather type classification, we only consider the parameter “mean sea level pressure” for a subset of quality-checked GCM runs, that are depicted in table 1. Note that available GCMs are also limited by their calendar, because a “Gregorian”-like calendar is a prerequisite for the calculation of weather types (please refer to the description of the COST733 software in the methodology section for further details). Hence, a subset of GCMs that would in principle be available, cannot be used because they employ other calendars. Furthermore, this table is subject to updates in the near future, as more data will become available.

Table 1: Overview of used GCM data for the calculation of weather types and the frequency and intensity analysis.

Model	Ensemble-member	Historical	SSP1-2.6	SSP3-7.0
ACCESS-CM2	r1i1p1f1	x	x	x
CNRM-CM6-1	r2i1p1f2	x	x	x
	r3i1p1f2	x	x	x
CNRM-CM6-1-HR	r1i1p1f2	x	x	x
CNRM-ESM2-1	r1i1p1f2	x	x	x
IPSL-CM6A-LR	r1i1p1f1	x	x	x

	r2i1p1f1	x	x	x
	r3i1p1f1	x	x	x
	r4i1p1f1	x	x	x
	r14i1p1f1	x	x	x
MIROC6	r1i1p1f1	x	x	x
MPI-ESM1-2-HR	r1i1p1f1	x	x	x
	r2i1p1f1	x	x	x
MRI-ESM2-0	r1i1p1f1	x	x	x

○ DAMAGE DATA

Combining the damage data sets of the WLV (WLK) and GBA (GEORIOS) for Austria with those of the IFFI and the ED30 database for South Tyrol and subsequently applying the translation scheme of the established vocabulary (please refer to D2.1 for further details) results in the so-called "event space". The event space covers the period from 1961 to 2021 and stretches over Carinthia and East Tyrol in Austria as well as South Tyrol (Alto Adige) in Italy.
This newly established database includes 1302 events on the Austrian side; 672 of them describe flood events, 633 entries relate to mass movements – flows and slides. In the case of South Tyrol, the event space comprises 623 flood events and 2229 mass movements. All events comprised in the event space feature an exact location in time and space. This is the prerequisite for both our analyses, i.e., the derivation of HTPs/HDCs and to a lesser extent for the linkage to weather types (exact location in space would not be needed for the latter).

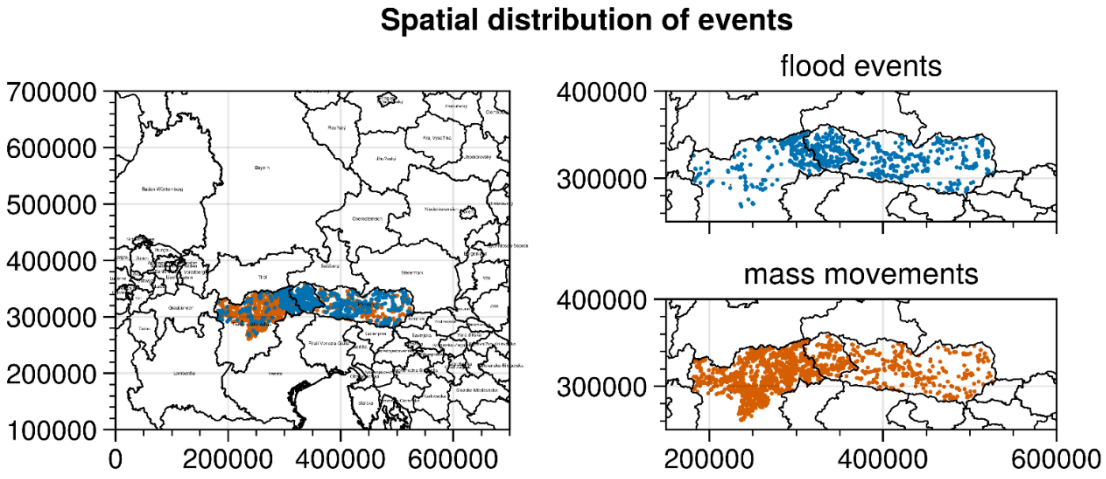

Figure 1.: Spatial distribution of flood events (blue) and mass movements (orange) in the target regions Carinthia/East Tyrol and South Tyrol.

3. METHODOLOGY

The methodology applied in this deliverable roughly consists of four major steps. The first deals with the identification of daily weather types in the past period from 1961 to 2020 for the Central European region using the COST733 weather type classification software (Philipp et al., 2014). In the second step, we determine future weather types using an ensemble of CMIP6 data. Subsequently,

we intersect aforementioned damage data with observed weather types on the respective event dates and receive a distribution of weather types that are connected to damage events. Lastly, we evaluate the changes in terms of both frequency and intensity for those weather types, by determining their change in terms of occurrence for frequency and by calculating various precipitation metrics associated to each weather type based on downscaled projections (see deliverable D2.4 for details on the downscaling scheme).

○ COST733 WEATHER TYPE CLASSIFICATION

For the determination of daily weather types in the past as well as the future, we use the so-called "cost733class" weather type classification software package (Demuzere et al., 2011; Philipp et al., 2014). This FORTRAN package focuses on both the creation as well as evaluation of weather and circulation type classifications using different methods. cost733class is released under GNU General Public License v3 (GPL) and freely available. Since the software was released in 2014, there are possibilities that it cannot deal with the newest reanalysis and GCM data, respectively. Therefore, extensive data preparation is necessary. For that purpose, it is essential to use the CDO[1] version 1.6.4 and the C-compiler version gcc4.8.5. Unfortunately, both packages cannot be installed or compiled on the newest Ubuntu version; hence, it is necessary to have a virtual machine (or a docker container) with Ubuntu 16.04 running on it. Moreover, the pre-processing only is successful when using models that feature a Gregorian calendar. Further technical details on the use of the "cost733class software" can be found in the COST733 User Guide by Philipp et al., 2014.

GWT WEATHER TYPE CLASSIFICATION

The cost733class software comprises various classification methods. Within this deliverable, we analyse the method "GWT" using solely mean sea level pressure. This method uses three prototype patterns and calculates the three Pearson correlation coefficients between each field in the input file and the three mentioned protypes (Beck et al., 2007). The first prototype represents a strict zonal pattern with values rising from north to south, the second is a strict meridional pattern with values increasing from west to east. The third pattern exhibits a cyclonic pattern with a minimum in the center and increasing values to the margin of the field. Depending on the three correlation coefficients and their combination, each input field is assigned to a class. Since there is only a fixed number of combinations, not all numbers of types can be reached. This method is useful only for single pressure fields. The possible numbers of types are: 8, 10, 11, 16, 18, 19, 24, 26, 27. For 8 types the main wind sectors (N, NE, E, SE, S, SW, W, NW) are used. Two additional types for purely cyclonic and purely anticyclonic situations result in 10 types and one indifferent type depending on cyclonicity leads to 11 types. For 16 types the following numbers apply: 1-8=cyclonic, 9-16=anticyclonic and for 24: 1-8=cyclonic, 9-16=anticyclonic, 17-24=indifferent. Adding 2 or 3 cyclicity types gives 18 or 19 and 26 or 27 types. For our analyses, we utilize 18 different types.

○ CLIMATE CHANGE ASSESSMENT

For the climate change assessments, we first identify the prevailing weather type for each day in the period from 1961 to 2020 by using the above introduced COST733 weather type classification

[1] https://code.mpimet.mpg.de/projects/cdo/

software. For this endeavour, we use mean surface level pressure fields from ERA5. The output of the cost733class software yields a time series of weather types with a daily resolution. The observed weather type time series is subsequently intersected with the existing damage data in the target regions, allowing us to determine specific weather types that potentially lead to higher levels in damage events than others. In order to assess changes under different climate scenarios, weather types are also calculated for mean sea level pressure fields from GCMs.

Before focussing on the climate change assessment, the most "critical" or high-impact weather types must be identified. For that purpose, we investigated the distribution of weather types prevailing on days, where damages were registered in the "event space". The two categories mass movements and floods are investigated separately, but each category for both regions of interest together. The GWT weather types for damage records are furthermore normalised with the observational frequency of weather types, in order to account for the non-equal distribution of observed weather types. Subsequently, we investigate the mean sea level pressure fields from ERA5 for the identified weather types and select those that are meteorologically the most meaningful for the European alpine region.

CHANGES IN FREQUENCY

For the determination of changes in the frequency of selected weather types, we evaluate their occurrence in two different future time periods. We thereby consider an ensemble of CMIP6 data, comprising two socio-economic pathways, SSP1-2.6 and SSP3-7.0. The first time period refers to the so-called 'near future', spanning from 2036 to 2065, whereas the second time period, the 'far future' stetches from 2071 to 2100. Changes in frequency are depicted as percentage changes relative to the frequency over the historical period of GCMs from 1950 to 2014.

CHANGES IN INTENSITY

To evaluate changes in intensity, we focus on two points: (i.) the potential precipitation increase caused by higher atmospheric temperature and (ii.) the change of different precipitation metrics calculated for days corresponding to specific weather types. In both cases the baseline was determined by historical GCM simulations and a reference period from 1961 to 1990 and the changes were calculated for both scenarios SSP1-2.6 and SSP3-7.0.

For the first approach we identify the mean temperature change over Europe and estimate the intensity change by using the Clausius-Clapeyron relationship. As a representation of atmospheric temperature, the air temperature at the 850 hPa level is used. For the area-means over Europe, the following bounding box has been considered: 32.5°N to 67.5°N and 10°W to 25°E. The area-averaged time series is then averaged per GCM ensemble member and time period (near future and far future, 2036 to 2065 and 2071 to 2100, respectively).

The second aim, evaluating the intensity change corresponding to different weather types, is conducted by extracting precipitation totals for days on which respective weather types prevailed. Subsequently, the mean over time and space for a given subset of days corresponding to a specific

weather type, the 95th percentile of time and space and the 95th percentile of area-means are calculated and evaluated. The changes of the GCM ensemble are then again analysed in the context of the two already outlined scenarios and time periods.

○ Hazard Development Corridors

The calculation of HDCs is delineated in Deliverable D2.4 in more detail. In essence, the EOF space constructed by the HTPs is used and precipitation totals from GCMs are projected into that space, yielding pseudo principal components. An observational-determined threshold is then used to determine the number of potential events in a given time series. The changes of potential events from a historical period to potential future time periods are then normalised with the historical period, yielding the HDCs.

4. Results

○ Hazard Development Corridors

The HDCs for all parameter combinations are shown in Figures 2 and 3 (two categories, two regions and four seasons). As already outlined, new data was included in this analysis, which is why the HDCs for the region ET_C are displayed again. The multi-model mean boxplots in Figure 2 show indistinct behaviour, where for some parameter combinations a slight decrease in the frequency of potential events is depicted, or for others a slight increase. Notables are furthermore the large variances for e.g., flood in ST for MAM and mass movement in ST for DJF and some cases with a changing tendency between the two time periods for the same experiment, e.g., flood in ST for MAM again. This may also indicate that the analysis for these parameter combinations is not robust enough for high confidence. Nevertheless, for other parameter combinations the shifts are more pronounced, indicating robust shifts or increased potential for higher severity of potential event frequencies. The change of the 90th percentiles indicate largely the same as the change of the means, namely indistinct shifts toward slightly less, or slightly higher frequency of potential events, depending on the category, region and season of interest. In terms of hazard potential, it has to be noted though, that even if the median (black horizontal line of boxplots) shows close to no change, this still means that 50% of the GCM ensemble show increasing hazard potential, or in other words there is a 50% chance of increased hazard frequency risk.

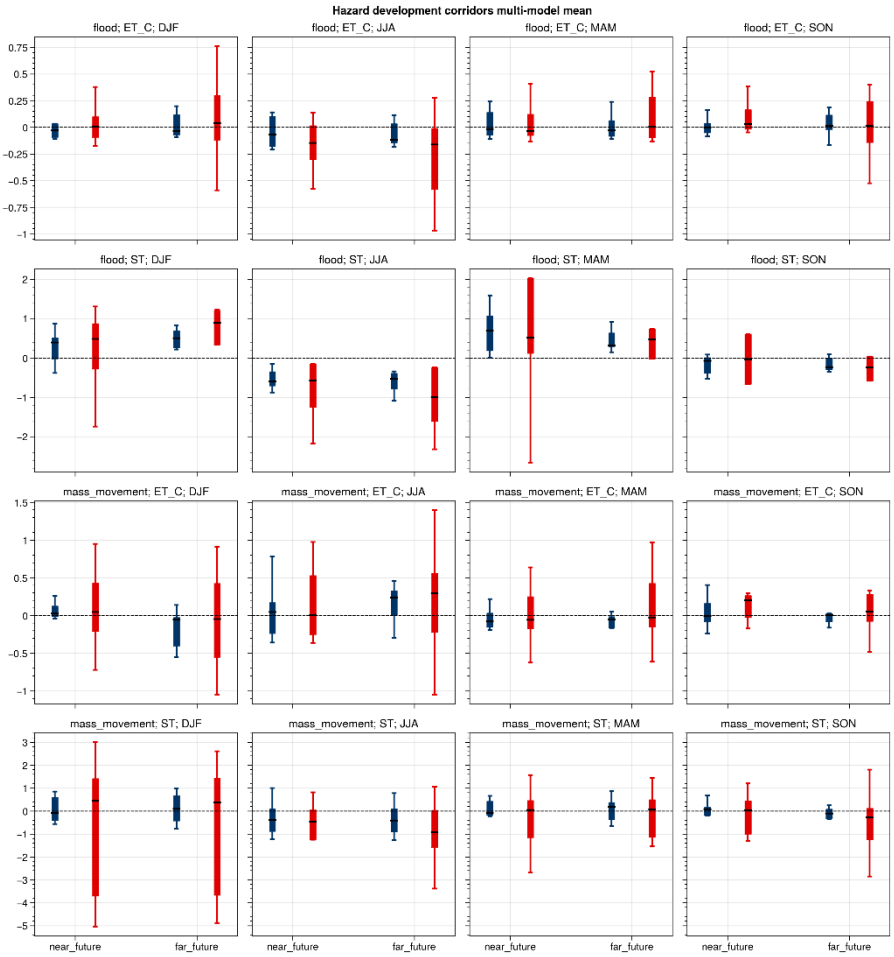

Figure 2: HDCs in terms of the change of the mean for the multi-model ensemble from historical to future time periods. Each subplot depicts on parameter combination for category (flood and mass movement), region (ET_C = East Tyrol and Carinthia, and ST = South Tyrol) and season (DJF, JJA, MAM, SON; winter, summer, spring and fall respectively). Each subplot shows two columns of boxplots with each column depicting two boxplots. The left column represents the “near future” (2036-2065) and the right one “far future” (2071-2100). In each column the left boxplot is for SSP1-2.6 (blue), the right for SSP3-7.0 (red).

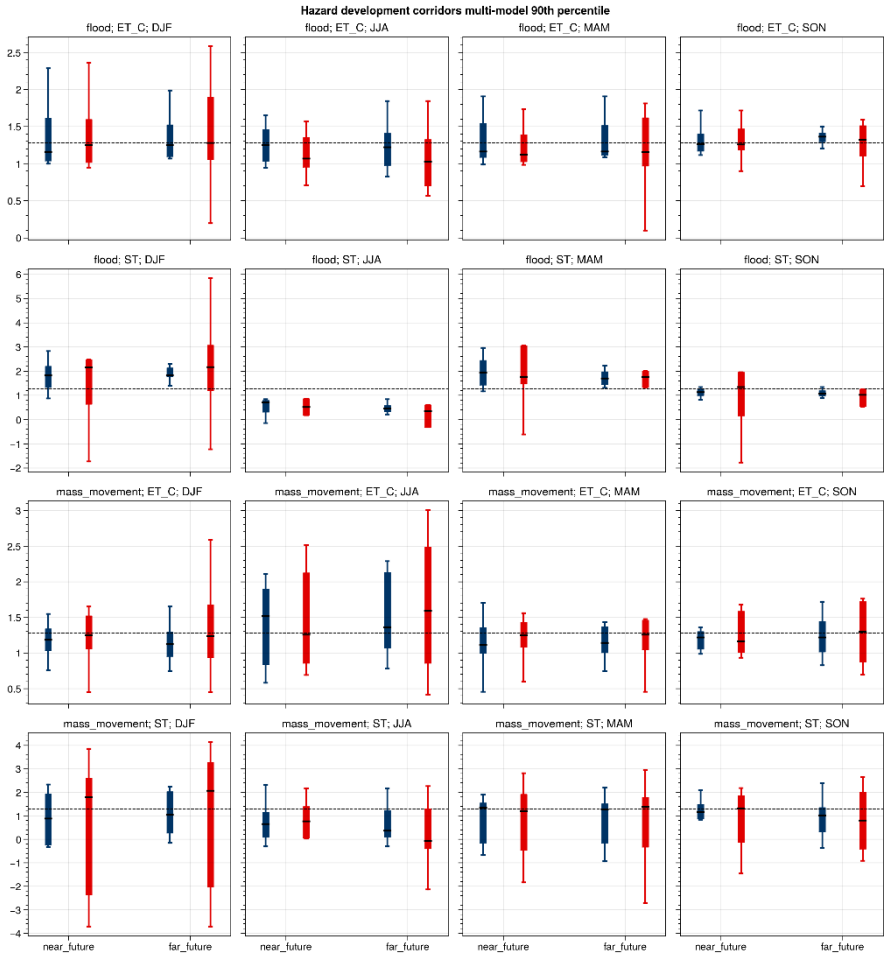

Figure 3: HDCs in terms of the change of the 90th percentile for the multi-model ensemble from historical to future time periods. See Figure 2 for an explanation on the figure structure.

○ WEATHER TYPES IN THE PAST

WEATHER TYPES IN ERA5

Before linking identified GWT weather classes to damage events, we investigate the distribution of all 18 classes in the period 1961 to 2020 in the ERA5 data. Figure 4 illustrates the relative values of the occurrence of different weather types. We thereby differentiate the period 1961 to 1990, depicted on the left panel as well as the period 1991 to 2020, shown on the right side, in order to assess the variability over the observational time period. Both time periods feature similar characteristics: the most prevailing weather types are the classes 1, 9 and 18. Class 1 represents a cyclonic pattern, whereas types 9 and 18 describe anticyclonic conditions over Central Europe. Differences in the distribution between the periods considered can hardly be detected; GWT 1 slightly decreases in the latter period, whereas the occurrence of GWT classes 10, 13 and 18 feature a weakly pronounced increase.

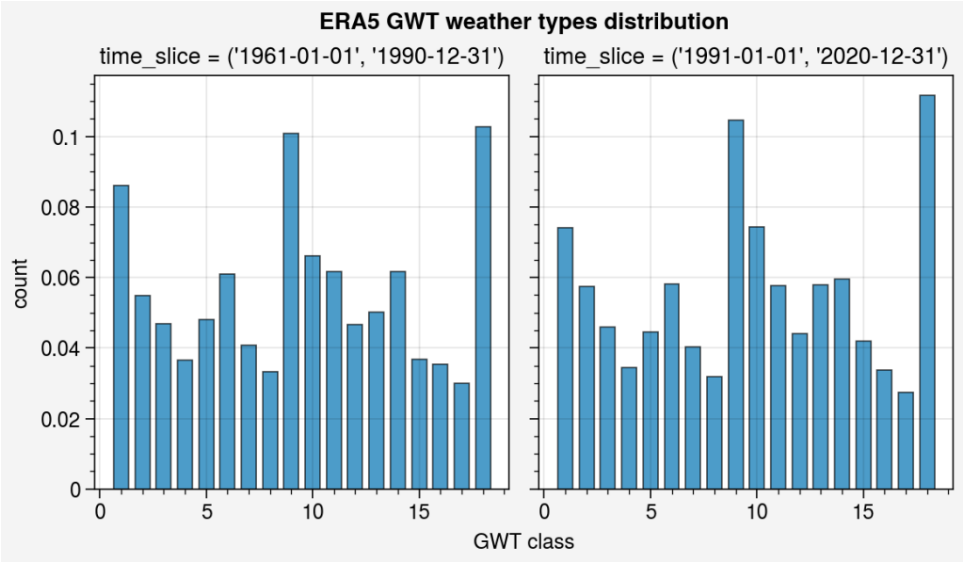

Figure 4: Distribution of the relative occurrence of 18 GWT weather types for the ERA5 reanalysis data, investigated for two 30-year-windows within the time period from 1961 to 2020. The left panel shows results for 1961 to 1990, the right side for 1991 to 2020.

LINKAGE OF GWT WEATHER TYPES AND DAMAGE RECORDS

In order to link the weather types to high-impact weather, we intersected the observed weather type time series with damage events that were registered in the "event space" (refer to section "damage data"). Figure 5 illustrates the distribution of GWT weather times prevailing on days where damage events were recorded, normalised with the observational frequency – to account for the non-equal distribution of observed weather types. With regards to mass movements, three GWT weather types stand out: 2, 8 and 17. In the case of floods, however, GWT 9 and 13 show relatively the highest occurrences. GWT 2 exhibit in both cases a high count.

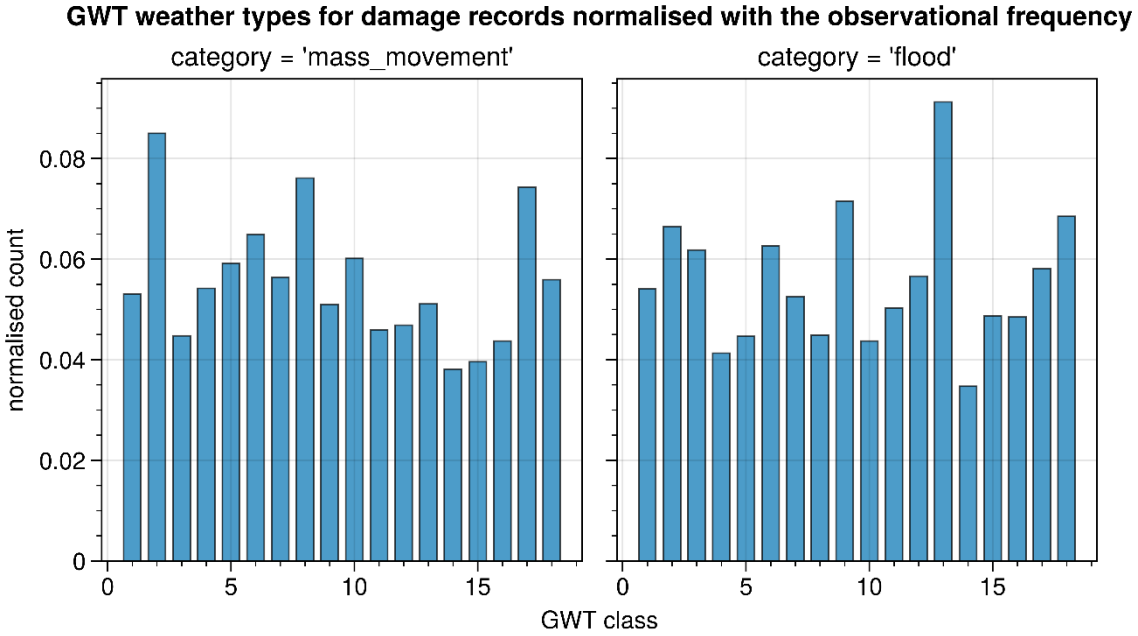

Figure 5: Distribution of GWT weather types prevailing on days when damage events were documented. The left panel shows results for the hazard category "mass movement", the right side reveals outcomes for the hazard category "floods".

If we now investigate the mean sea level pressure field for the GWT weather types identified, illustrated in Figure 6, i.e., the types 2, 7, 8, 10, 13 and 17, it can be seen that types 2, 7 and 8 represent cyclonic weather situations with a high-pressure field over the Azores and a corresponding low over the north of Europe. This low-pressure area has different intensities in the different weather classes as well as spatial extensions to Central Europe. The weather pattern represented by GWT 2 and 8 exhibit a strong cyclonic influence in Central Europe, whereas the gradient over Central Europe is weaker when considering GWT 7.

On the contrary, GWT 10 and 13 show anticyclonic conditions over Central Europe, characterized by a high-pressure field that stretches from the Azores to the European alpine region. These weather types may entail favourable conditions for convective events that potentially lead to small-scale high-impact weather events.

According to the GWT classification scheme with 18 different classes, GWT 17 represent the so-called 'cyclonicity'. This pressure field is characterized by a pronounced low-pressure system over the European alpine region.

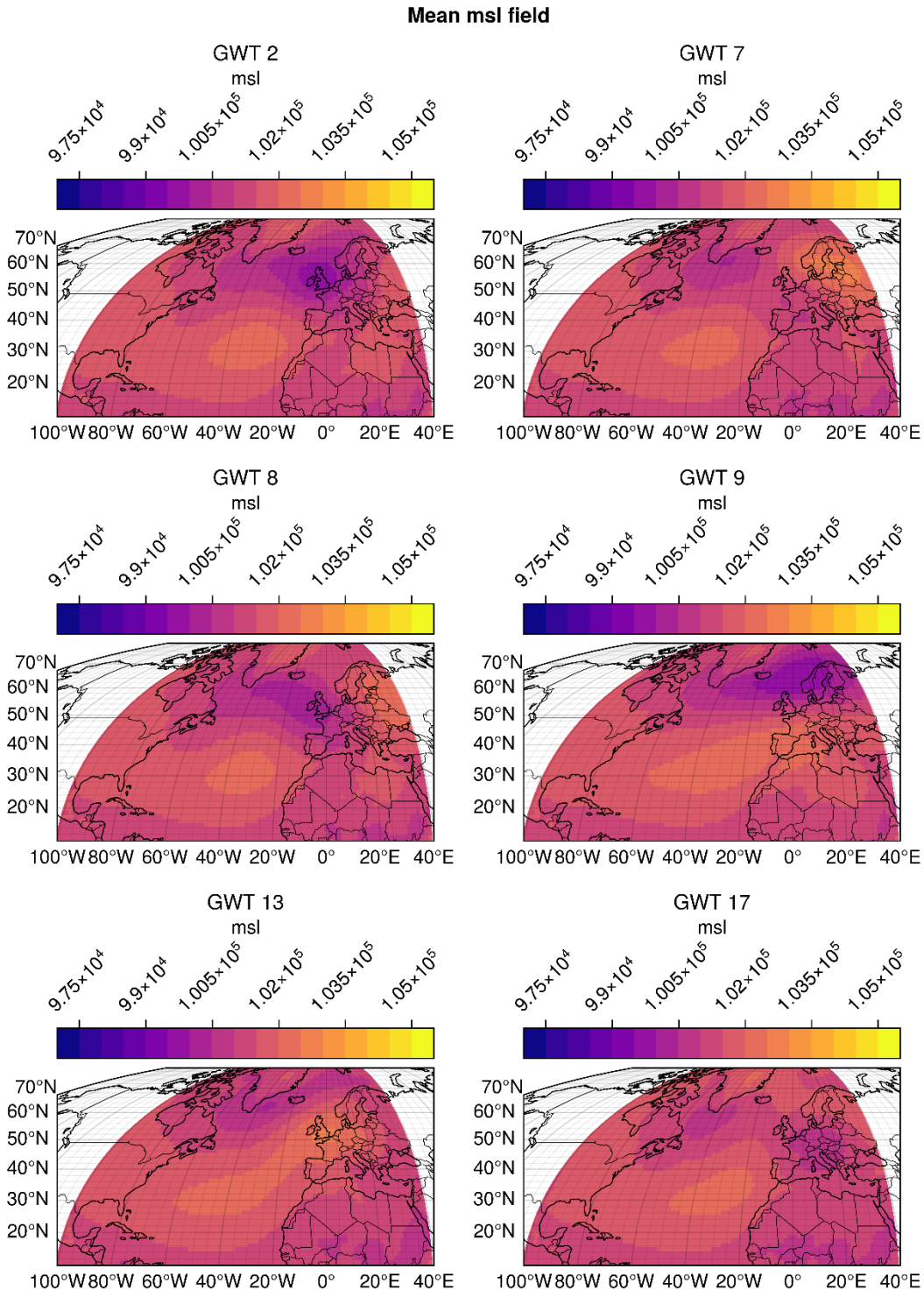

Figure 6: Fields of mean sea level pressure for identified GWT classes from ERA5. GWTs 10 and 13 refer to anticyclonic conditions over Central Europe whereas GWT classes 2, 7, 8 and 17 represent cyclonic conditions over the European Alps.

GWT weather classes of Vaia

GWT classes 2 and 7 are also the weather types that were prevailing during the Vaia event in 2018. The meteorological conditions during the period from October 28th to 30th can be summarized as followed: in the evening of October 26th, 2018, a trough of low pressure strengthened over the western Mediterranean Sea, which led air masses from the Mediterranean Sea to the northeast and could strengthen into a vortex – called Vaia. This vortex remained more or less stationary due to

blocking high-pressure systems both to the east as well as west and just slowly moved towards North in the following days; the counter-clockwise rotation allowed large amounts of evaporative moisture to be absorbed over the warm Mediterranean Sea, which lead to heavy rainfall in northern Italy, the southern parts of Austria as well as parts of Switzerland. The sea level pressure field as well as the 500 hPa geopotential height on October 29th, 2018 can be seen in Figure 7. On this day, the core of the low-pressure system was over the Mediterranean Sea. The same situation is described in the GWT class 7 and to a lesser extent, but still comparable, in GWT 8 (see Figure 6). Hence, taking into account the observational frequency of weather types as shown in Figure 4, the weather type preconditioning for "Vaia"-like events is on the lower end of the observed distribution of weather types for GWT 7, 8 and around the average for GWT 2. However, linking the weather types to damage records decisively shows, that those weather types are associated with relatively higher impact and are therefore of special interest to investigate for potential changes.

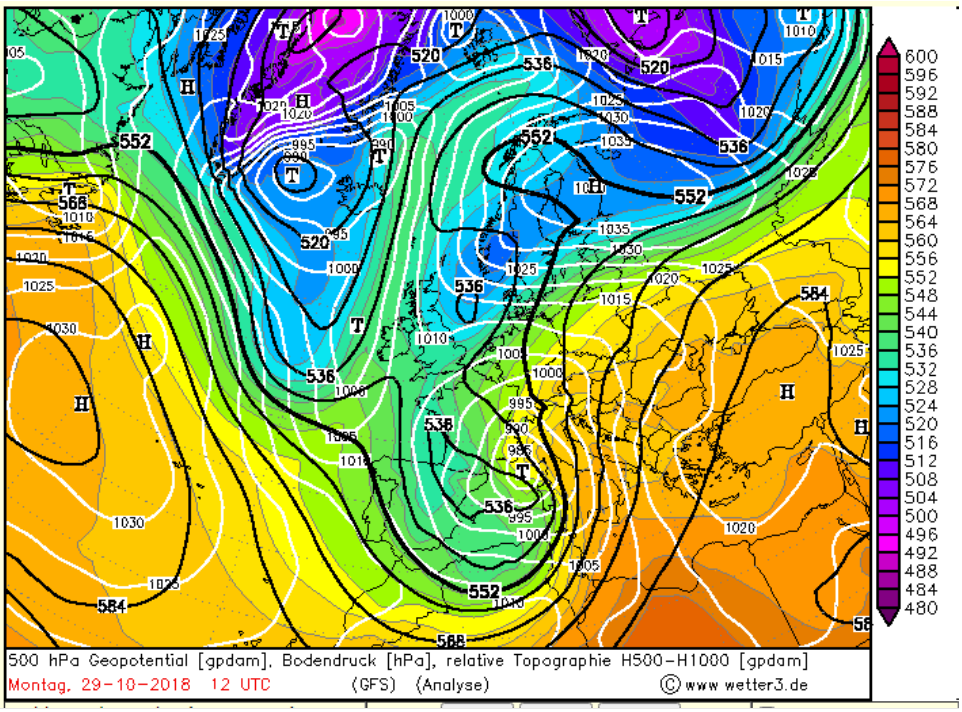

Figure 7: Mean sea level pressure field (white) and 500 hPa geopotential height (black) as well as the relative topography (color-coded) for October 29th, 2018, 12 UTC (source: wetter3.de).

○ WEATHER TYPES IN THE FUTURE

CHANGES IN FREQUENCY

Results for IPSL-CM6A-LR

Figure 8 shows the changes in frequency for all 18 GWT classes for SSP1-2.6 (blue) as well as SSP3-7.0 (red) for both the near and the far future for the model IPSL-CM6A-LR, r3i1p1f1. It can be seen that the occurrence of some weather classes decreases while others increase. In some cases, however, the different scenarios reveal different tendencies. Overall, values of percental change reveal magnitudes with maxima around 20% in both directions. Outcomes for the far future, as depicted on the right panel, reveals a much more pronounced picture with vastly higher percentage changes. In this case, magnitudes are profoundly higher for SSP3-7.0 than for SSP1-2.6. This is not surprising,

since those two scenarios are quite similar for the first half of the century, whereas differences between them evolve and grow in the second half.
The high-impact weather types GWT 2, 8 and 17 reveal a rise in occurrence frequency which is, however, not of the same magnitude. GWT 2 shows an increase in frequency of 10% considering SSP3-7.0, whereas GWT 8 features a rise of nearly 30%. The occurrence of GWT 17 also increases by 20%. These values need to be taken with a grain of salt though, as they represent only the outcome of one model run, which inherently contains a large variability component.

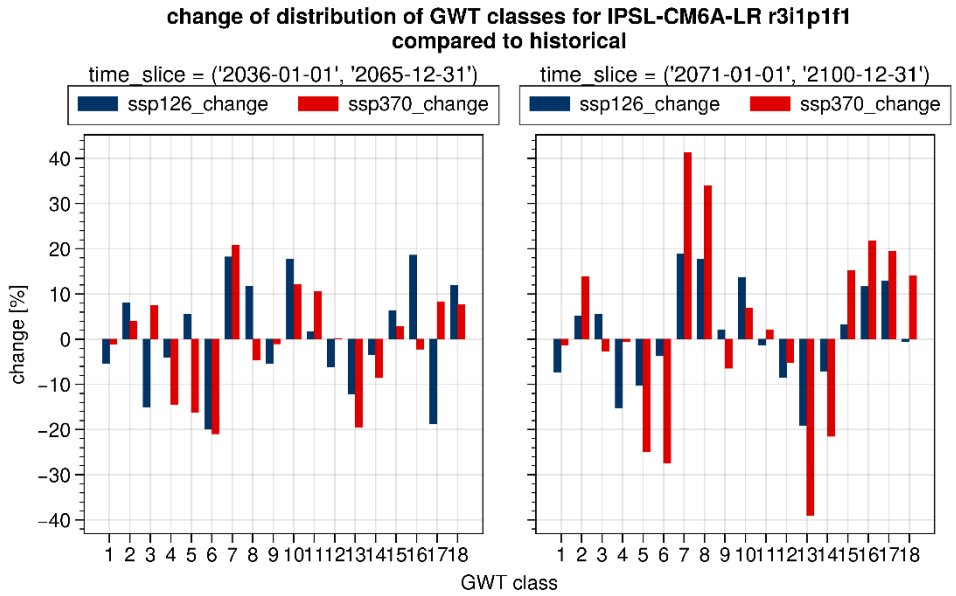

Figure 8: Changes in frequency for all 18 GWT weather classes when considering the model IPSL-CM6A-LR, run r3i1p1f1 for scenarios SSP1-2.6 (blue) and SSP3-7.0 (red) for the near (left) as well as for the far future (right).

Results for a three-member ensemble

Figures 9 and 10 refer to changes in frequency of the 18 GWT weather classes under consideration of a three-member ensemble. This ensemble comprises the above described 'IPSL-CM6A-LR' (run: r3i1p1f1), the 'MIROC6' model (run: r1i1p1f1) and the 'CNRM-ESM2-1' model (run: r1i1p1f2). Results for SSP1-2.6 and SSP3-7.0, respectively, are again separated in the two assessment periods, i.e., the near and the far future.
Outcomes for SSP1-2.6 reveal that approximately half of the 18 GWT weather classes experience an insignificant amount of change compared to the variability across the GCMs. However, especially the high-impact weather classes GWT 2, 8 and 17 and the VAIA-prevalent weather type GWT 7 show a substantial increase in frequency, with changes slightly more pronounced in the far future, where increased frequencies are about 10 to 20%.
Figure 10 reveals overall the same characteristics for SSP3-7.0, but contrary to SSP1-2.6 the weather type GWT 2 shows no substantial increase, which on a sidenote was also the one type with the smallest increase in SSP1-2.6. On the flipside, GWT 7 and 8 show much larger increases in frequencies, especially toward the end of the century, with the upper limit for those types depicting increases of 30 to 40%. Especially striking is the fact that all considered models show a significant increase for those two types, even though there is still some variability in the precise magnitude.
In general, the uncertainty which stems from the small ensemble is – depending on the weather class investigated – still high compared to the median of the change, which indicates an insignificant change. However, especially the weather types that are associated with damage records – GWT 7, 8 and 17 – show significant increases and therefor increasing frequencies for potential high-impact

weather events. The analyses will evolve and grow more robust as the considered ensemble is subject to increase.

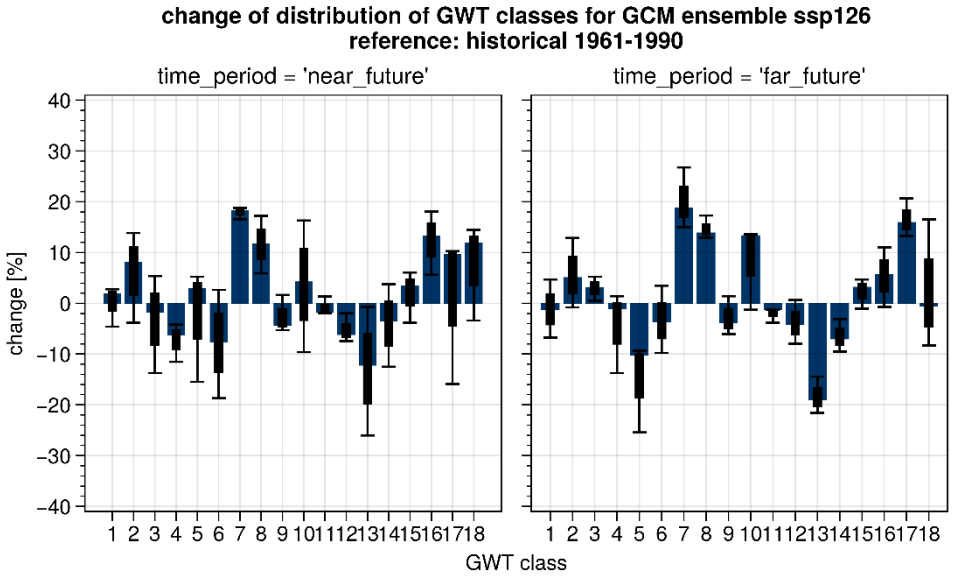

Figure 9: Distribution of changes of GWT classes for the considered GCM ensemble for SSP1-2.6 compared to the historical period.

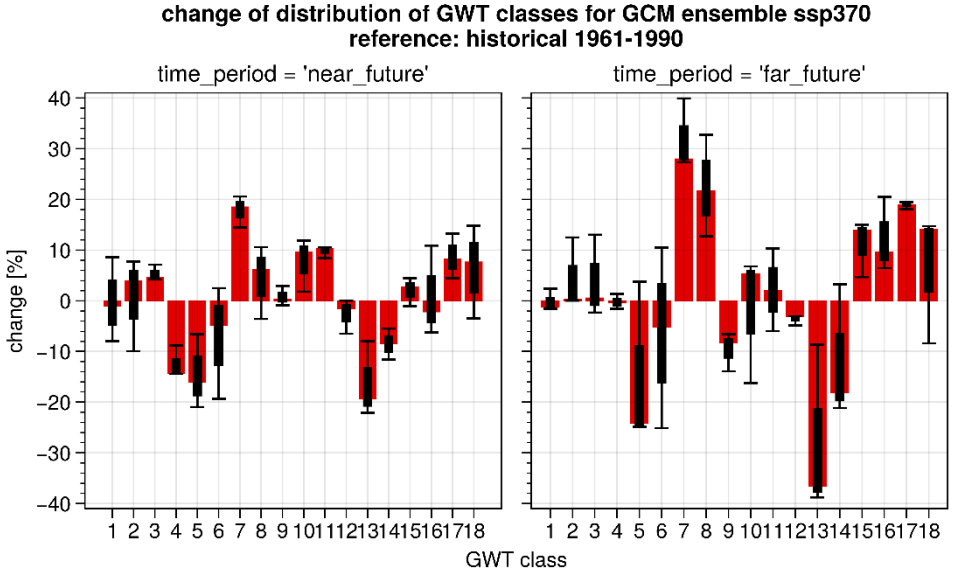

Figure 10: Distribution of changes of GWT classes for the considered GCM ensemble for SSP3-7.0 compared to the historical period.

CHANGES IN INTENSITY

i. Estimation of temperature change using the Clausius-Clapeyron relationship

The first approach consists of linking the mean temperature rise over Europe to the change in rainfall intensity by using the Clausius-Clapeyron equation. This relationship indicates that 1°C temperature rise leads to 7% more precipitation.

Figure 11 depicts the results for the 850 hPa temperature change, based on a multi-model ensemble with 99 members, which was taken from the available list of GCMs that was subject to the GCM evaluation in deliverable D2.4, to get the most robust estimate.
Temperature increases for both considered scenarios are similar in the near future, showing a median of around 3°C, but the SSP3-7.0 scenario exhibits more pronounced distribution overall. By using the Clausius-Clapeyron relationship, this temperature rise leads to potentially 21% more precipitation in Europe for the median of the GCM ensemble.
Temperature rise remains roughly the same for the climate-friendly SSP1-2.6 in the far future with only a slight increase. However, SSP3-7.0 shows a much more pronounced temperature increase and reaches almost 5.5°C, in terms of the median, at the end of the century. This warming would indicate a potential increase of up to 38.5% in precipitation.

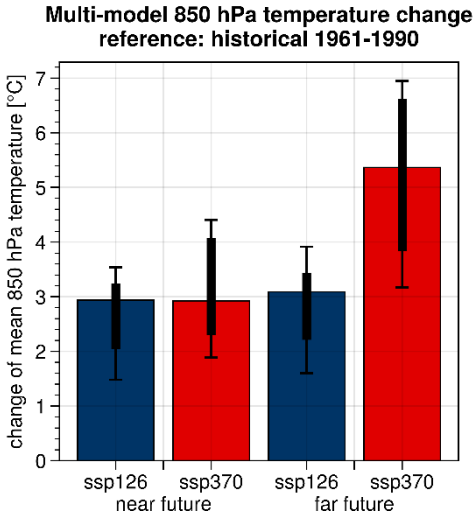

Figure 11: Multi-model 850 hPa temperature change in Europe with respect to the time period 1961 to 1990. Blue bars indicate results for SSP1-2.6, red bars for SSP3-7.0. Assessments have been made for the near (left side) as well as far (right side) future. The underlying ensemble consists of 99 members.

ii. Calculation of precipitation intensity changes based on downscaled precipitation data

The second approach consists of extracting daily precipitation values for the target region from downscaled GCM data. Analyses have been conducted also for the near and far future. Figure 12 reveals outcomes for SSP1-2.6 (blue) and SSP3-7.0 (red) in the near (top two rows) and far (bottom two rows) future. The first column represents the change in percentage of mean precipitation over time and space for a subset of days corresponding to a specific weather type. The middle column shows the 95th percentile over time and space and the third column shows the 95th percentile of area-averaged precipitation totals.
Preliminary results show inconclusive intensity changes for GWT 2, 8, but a tendency for pronounced increased intensities for GWT 7 and 17. The inclusion of more model data will yield a more robust analysis, after which final remarks and conclusions can be drawn.

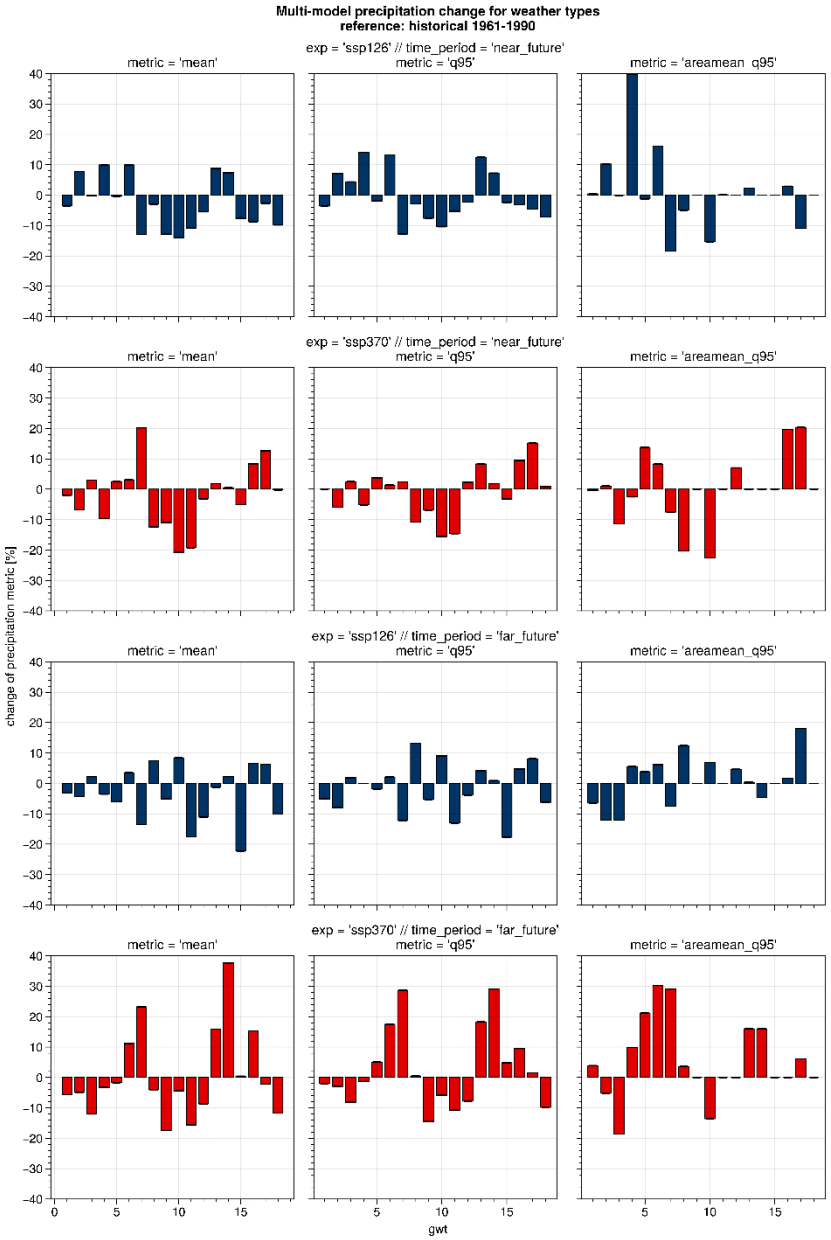

Figure 12: Change of precipitation metrics for the combined regions of ST and ET_C for the model IPSL-CM6A-LR r3i1p1f1 for the two scenarios and time periods in question, with respect to the time period 1961 to 1990 from the historical model simulations. Blue bars indicate results for SSP1-2.6, red bars for SSP3-7.0. The first two rows indicate the change for the "near_future", the latter two for the "far_future". Note: This figure will be updated with more model data and will ultimately represent the results for the GCM ensemble.

5. References

Beck, C., Jacobeit, J., and Jones, P. (2007): Frequency and within-type variations of large scale circulation types and their effects on low-frequency climate variability in central europe since 1780. *Int. J. Climatol.*, 27, 473–491. https://doi.org/10.1002/joc.1410

Copernicus Climate Change Service (C3S) (2017): ERA5: Fifth generation of ECMWF atmospheric reanalyses of the global climate. Copernicus Climate Change Service Climate Data Store (CDS), *date of access*. https://cds.climate.copernicus.eu/cdsapp#!/home

Demuzere, M., Kassomenos, P., and Philipp, A. (2011): The COST733 circulation type classification software: an example for surface ozone concentrations in Central Europe. *Theor. Appl. Climatol.,* 105, 143–166. https://doi-org.org/10.1007/s00704-010-0378-4

European Environment Agency (EEA) (2016): Climate change, impacts and vulnerability in Europe 2016 – An indicator based record, ISBN: 978-92-9213-835-6

Feyen, L., Dankers, R., Bódis, K., Salamon, P., and Barredo, J. I. (2012): Fluvial flood risk in Europe in present and future climates. *Climatic Change*, 112, 47-62. https://link.springer.com/article/10.1007/s10584-011-0339-7

Hersbach, H., Bell, B., Berrisford, P., et al. (2020): The ERA5 global reanalysis. *Q. J. R. Meteorol. Soc.,* 146, 1999–2049. https://doi.org/10.1002/qj.3803

IPCC, 2014: *Climate Change 2014: Synthesis Report. Contribution of Working Groups I, II and III to the Fifth Assessment Report of the Intergovernmental Panel on Climate Change* [Core Writing Team, R.K. Pachauri and L.A. Meyer (eds.)]. IPCC, Geneva, Switzerland, 151 pp.

Philipp, A., Bartholy, J., Beck, C., Erpicum, M., Esteban, P., Fettweis, X., Huth, R., James, P., Jourdain, S., Kreienkamp, F., Krennert, T., Lykoudis, S., Michalides, S. C., Pianko-Kluczynska, K., Post, P., Alvarez, D. R., Schiemann, R., Spekat, A., Tymvios, F. S. (2010): Cost733cat - a database of weather and circulation type classifications. *Phys. Chem. Earth.*, 35, 360–373. https://doi.org/10.1016/j.pce.2009.12.010

Riahi, K., van Vuuren, D. P. , Kriegler, E., Edmonds, J., O'Neill, B. C., Fujimori, S., Bauer, N., Calvin, K., Dellink, R., Fricko, O., Lutz, W., Popp, A., Cuaresma, J. C., Samir, K. C., Leimbach, M., Jiang, L., Kram, T., Rao, S., Emmerling, J., Ebi, K., Hasegawa, T., Havlik, P., Humpenöder, F., Da Silva, L. A., Smith, S., Stehfest, E., Bosetti, V., Eom, J., Gernaat, D., Masui, T., Rogelj, J., Strefler, J., Drouet, L., Krey, V., Luderer, G., Harmsen, M., Takahashi, K., Baumstark, L., Doelman, J. C., Kainuma, M., Klimont, Z., Marangoni, G., Lotze-Campen, H., Obersteiner, M., Tabeau, A., and Tavoni, M. (2017): The Shared Socioeconomic Pathways and their energy, land use, and greenhouse gas emissions implications: An overview. *Glob. Environ. Change*, 42, 153-168. https://doi.org/10.1016/j.gloenvcha.2016.05.009